**Manuscript after review**

**Access to published version: https://www.sciencedirect.com/science/article/pii/S138358662100215X**

# Photo-assisted ozonation of cefuroximewith solar radiation in a CPC pilot plant. Kinetic parameters determination

Rafael R. Solís[1,*], Ana M. Chávez[2,3,*], Olga Monago-Maraña[2,3], Arsenio Muñoz de la Peña[3,4], Fernando J. Beltrán[2,3]

[1]Departamento de Ingeniería Química, Facultad de Ciencias, Universidad Autónoma de Madrid, Madrid, Spain

[2]Departamento de Ingeniería Química y Química Física, Facultad de Ciencias, Universidad de Extremadura, Badajoz, Spain

[3]Instituto Universitario del Agua, Cambio Climático y Sostenibilidad (IACYS), Universidad de Extremadura, Badajoz, Spain

[4]Departamento de Química Analítica, Facultad de Ciencias, Universidad de Extremadura, Badajoz, Spain

*To whom correspondence should be addressed: Rafael Rodríguez Solís (rafael.rodriguez@uam.es) and Ana M. Chávez (amchavez@unex.es).

**Abstract**

The combination of ozone and solar radiation can be considered an effective technology as advanced oxidation process, AOP, for addressing the removal of harmful contaminants of emerging concern in water. Cefuroxime is an example of an antibiotic whose presence may result in a problem if not conveniently removed from the water. Cefuroxime oxidation has been performed employing photolytic ozonation in an autonomous pilot plant, consisting of a solar collector photo-reactor with ozone feeding, solar panel cells, and batteries for energy demands. Firstly, the kinetics of cefuroxime ozonation has been deeply studied in an agitation cell reactor. The stoichiometric ozonation ratio was estimated as $z_{O3}$=1.00±0.06 ($O_3$ mol per cefuroxime mol) and the second-order rate constant in the range 1.50 x $10^6$ – 4.69 x $10^6$ $M^{-1}$ $s^{-1}$ for the non-dissociated and dissociated, respectively, cefuroxime molecule. The oxidation

intermediates identified included hydroxylation of the initial molecule, attack to the secondary amide group and oxidation of the bi-substituted sulfide position. Secondly, the simultaneous application of ozone and solar radiation in the CPC pilot plant enhanced the degradation of cefuroxime. The kinetics in CPC reactor was simulated and the importance of the hydroxyl radical over ozonation and photolysis was confirmed, 55% of HO• pathway. Also, over 55% of mineralization was observed during photolytic ozonation in wastewater matrix whereas single ozonation only was able to partially oxidize the initial organic content to short organic acids (formic, acetic, and oxalic) that were accumulated in the water.

**Keywords:** ozone, photolytic ozonation, cefuroxime, intermediates, CPC pilot plant

## Highlights:

- Cefuroxime ozonation develops in the fast instantaneous kinetic regime.
- Second-order rate constant with molecular $O_3$ within 1.50 x $10^6$ – 4.69 x $10^6$ $M^{-1}$ $s^{-1}$.
- Identification of the oxidation products during the ozonation of cefuroxime.
- Photolytic ozonation of cefuroxime at pilot plant scale with solar radiation.
- Photo-ozonation enhances the mineralization degree if compared to ozonation.

## Graphical abstract

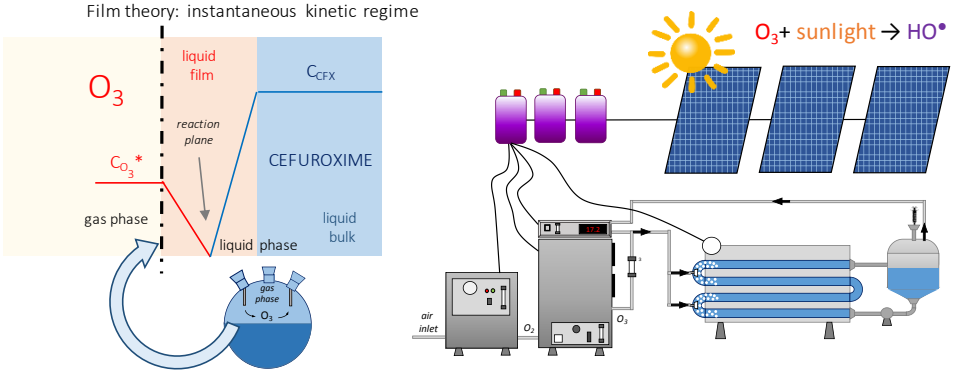

## 1. INTRODUCTION

The presence of antibiotics in the environment is a hazard of great concern since it contributes to the development of antimicrobial resistance and, therefore, loss of their efficiency in medical treatment. Current wastewater treatment plants are not designed to address the removal of these substances which aggravates the growth of resistance drawbacks [1]. Cefuroxime is a $\beta$-lactam antibiotic belonging to the second-generation cephalosporin family, used for the treatment of a wide range of infectious bacteria. The occurrence of cephalosporin antibiotics has been reported in wastewater at μg $L^{-1}$ and ng $L^{-1}$ level [2,3].

Currently, wastewater treatment plants need new specific designs to consider the presence of hazardous organic micropollutants, such as antibiotics, that need to be efficiently removed before being discharged to the environment [4]. Moreover, climate change is expected to force the reuse of wastewater for certain purposes as water availability and quality will be highly compromised in the early future.

Ozonation is a clean chemical oxidation technique that has been proved to be efficient and feasibly implemented as an extra stage in water treatment plants. Nevertheless, ozone reactivity towards organic micropollutants is selective, i.e. second-order rate constants vary in a really wide range from 0.1 to $10^9$ $M^{-1}$ $s^{-1}$ [5,6], and barely leads to great mineralization extent due to the recalcitrant nature of intermediates or final oxygenated organic acids. The chemistry of ozone in water involves the formation of hydroxyl radical, $HO^{\bullet}$, which reacts unselectively and with high rate constants, in the order of $10^7$-$10^{10}$ $M^{-1}$ $s^{-1}$, with almost all organic compounds. Accordingly, diverse ozone-based technologies have been proposed to promote the decomposition of dissolved $O_3$ into $HO^{\bullet}$ to raise the mineralization extent. From all of them, photolytic ozonation, e.g. combination of $O_3$ and radiation is an interesting technology since it

avoids the use of catalysts, whose removal from the water after treatment is still an unsolved problem, or the addition of extra hydroxyl radical promoters like $H_2O_2$. Although ozone presents a maximum of radiation absorption at 254 nm [7], which makes UVC the most suitable for that purpose; absorption in the visible spectrum [8] allows solar radiation to decompose $O_3$ to enhance $HO^{\bullet}$ production [9–11].

This study reports the use of ozone and solar radiation for the oxidation of the antibiotic cefuroxime in water. Ozonation kinetics of this antibiotic was first assessed since no data were available in the literature. A combination of simulated solar radiation and ozone was applied to cefuroxime elimination and mineralization. These results were also compared to real solar radiation, conducting tests of cefuroxime photolytic ozonation in a CPC-pilot plant, fed with renewable solar energy.

## 2. EXPERIMENTAL

### 2.1. Chemicals and materials

Cefuroxime sodium salt (CFX, $C_{16}H_{15}N_4NaO_8S$, CAS: 56238-63-2) was analytical grade acquired from Sigma-Aldrich®. All the chemicals used for analytical purposes were analytical grade and used as received. HPLC-grade acetonitrile was used in liquid chromatography. Ultrapure water from a Milli-Q® Integral 5 water purification system (resistivity 18.2 MΩ cm) was used for the preparation of all solutions.

Simulated Urban WasteWater (SUWW) was prepared following a recipe described in previous works without the addition of carbonate and phosphate anions [12–14]. The presence of these inorganic anions has been demonstrated to be negative for mineralization process [14] since both, the organic and inorganic content, compete for the reaction with hydroxyl radicals. Therefore, the inorganic carbon content was

removed to better study the direct reaction of cefuroxime with ozone. Table 1 shows the main parameters measured for the characterization of this simulated effluent.

**Table 1.** Characterization of the Simulated Urban WasteWater effluent

| Parameter | Value |
|---|---|
| TOC (mg $L^{-1}$) | 16.6 ± 0.2 |
| Chloride (mg $L^{-1}$) | 1.5 ± 0.2 |
| Sulfate (mg $L^{-1}$) | 11.5 ± 0.2 |
| Nitrate (mg $L^{-1}$) | 0.185 ± 0.006 |
| pH | 7.0 ± 0.5 |

### 2.2. Experimental setup and procedure

Preliminary ozonation tests were conducted in a semi-batch gas-liquid bubbled reactor, see Fig. 1A. Alternatively, the kinetics of cefuroxime ozonation was studied in a gas-liquid agitated cell reactor at different pH values. In both cases, a 500 mL spherical borosilicate glass reactor was filled in with 250 mL of the aqueous solution. The $O_2$-$O_3$ gas mixture ($Q_{GAS}$=30 L $h^{-1}$, $C_{O3,GAS}$=5 mg $L^{-1}$), generated in an Anseros COM-AD-01 device (Anseros, Germany), was fed to the water free interphase. The concentration of the ozone in the gas phase at the inlet or outlet of the reactor was monitored by an Anseros GM ozone analyzer (Anseros, Germany).

The stoichiometric ratio of the reaction between ozone and cefuroxime was determined by mixing (final volume, 5 mL) different aqueous solutions of cefuroxime and ozone, previously obtained by saturating ultrapure water with ozone. After mixing, the ratio of initial concentration, $C_{CFX,i}/C_{O3,i}$ moves to $C_{CFX,f}/C_{O3,f}$. The stoichiometric ratio ($z_{O3}$) is defined as the mol of $O_3$ consumed per mol of CFX reacted:

$$z_{O_3} O_3 + CFX \xrightarrow{k_{O_3,CFX}} P \quad (1)$$

$$z_{O_3} = \frac{C_{O_3,i} - C_{O_3,\mathrm{f}}}{C_{CFX,\mathrm{i}} - C_{CFX,f}} \quad (2)$$

The representation of $z_{O3}$ versus $C_{CFX,0}/C_{O3,0}$ leads to a hyperbolic curve whose horizontal asymptotic value corresponds to the $O_3$ mol per CFX mol consumed ($z_{O3}$) [15] (see later, section 3.1.1).

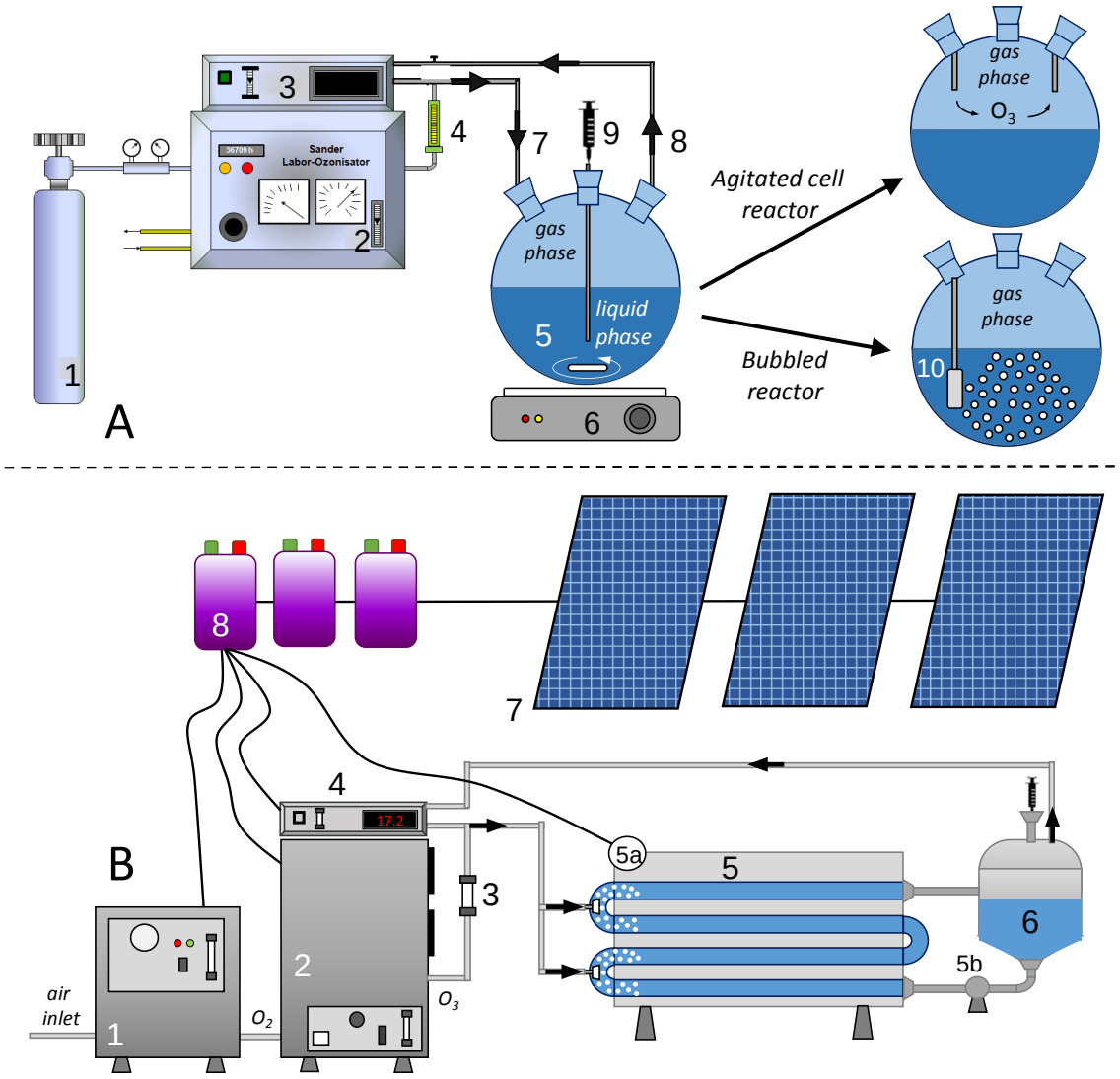


**Figure 1**. Experimental setups. **Gas-liquid reactor operating as agitated cell or bubble tank (A)**: pure oxygen tank (1), lab-scale ozone generator (2), gas-phase ozone analyzer (3), flowmeter (4), spherical cell glass reactor (5), magnetic stirrer (6), gas inlet (7), gas outlet (8), sampling point (9), ceramic diffuser (10). **Solar photo-ozonation pilot plant (B)**: pure oxygen generator from air (1) pilot plant ozone generator (2), flowmeter (3), gas-phase ozone analyzer (4), CPC-photo-reactor (5), radiometer (5a), recirculation pump (5b), gas-liquid separation tank (6), photo-voltaic panels (7), batteries (8).

The solar photo-assisted ozonation experiments at the pilot plant scale, see Fig. 1B, were carried out in a Compound Parabolic Collector (CPC) photo-reactor (developed by Ecosystem-Environmental Services S.A., Spain). The CPC photo-reactors are static collectors with a polished reflective surface built as an involute around a cylindrical pipe in which flows the aqueous solution. This display has found to provide a good optics for low concentration systems. Almost all the UV radiation arriving at the CPC surface, not only direct but also diffuse, is collected [16]. The CPC photo-reactor used in this work consisted of four tubes of 75 cm length and 30 mm internal diameter connected in series with a total gathering reflection surface of 0.25 $m^2$ (electro-polished aluminum) and a 5.0 L water treated volume (1.8 L illuminated). The irradiated surface is inclined 45º to the horizontal, i.e. approximately the latitude of the local place, for maximum radiation use. Moreover, each tube was located in the involute axis of the reflection surface producing a concentration factor near 1 and a radiation acceptance semi-angle of 90º. This CPC photo-reactor prototype was designed for bubbling a mixture of $O_2$-$O_3$ in the joints of the tubes through ceramic diffusers. The CPC reactor works in recirculation mode from a gas-liquid separator from which a pump sends the water to the tubes at a rate of 8 L $min^{-1}$. For ozonation requirements, firstly purified oxygen was produced from the air with an oxygen purifier (GENOX4, Cosemar Ozono S.A., Spain; 5 L $min^{-1}$ maximum) and secondly fed to an ozone generator (SP MILLENIUM 32 GR, Cosemar Ozono, Spain; 32 g $O_3$ $h^{-1}$ maximum). The flow rate of the $O_2$-$O_3$ mixture was adjusted in a flowmeter and send afterward to the ceramic diffusers located in the CPC ($Q_{GAS}$= 30 L $h^{-1}$; $C_{O3,inlet}$=15 mg $L^{-1}$). Ozone concentration in the gas phase was monitored in the inlet and the outlet of the CPC, from the separation tank, with a gas-phase ozone analyzer (Anseros GM, Anseros, Germany). The electricity energy requirements for ozone gas generation and analysis, pump and

CPC photo-reactor were supplied by 30 solar photovoltaic modules (260W and 60 cells each, polycrystalline, Inversolar S.L., Spain) connected to 24 batteries (PowerSafe® TS battery OPzS HYT-6P, 912 Ah, EnerSys®, USA). The installation provided a maximum energy capacity of 13.5 kWh per day with 1.3 days of autonomy.

The global direct and diffuse UV radiation was monitored with time through a UV radiometer ACADUS85-PLS (Ecosystem-Environmental Services S.A., Spain), located in the corner of the CPC. Thus, the accumulated UV irradiated energy was calculated by monitoring the temporal evolution of UV radiation reaching the CPC reactor surface [17]:

$$Q_{UV,T} = \frac{A_{tube} \times f_G + A_{CPC} \times f_G \times f_{T.}}{V_T} \int E_{UV}(t)dt \qquad (3)$$

where $Q_{UV,T}$ is the accumulated energy per volume of treated water (kJ $L^{-1}$), $E_{UV}(t)$ the punctual value of radiant flux received by the surface per unit area at a certain time (W $m^{-2}$), $A_{tube}$ is the irradiated surface area of the pipes, $A_{CPC}$ is the total irradiated area of the CPC and $V_T$ the total aqueous volume of the photo-reactor. The parameters $f_G$ and $f_T$ are, respectively, correction factors that account for the borosilicate glass transmittance ($f_G$=0.9) and the aluminum reflectance ($f_T$=0.686) provided by the manufacturer of the solar photo-reactor. Discussion of results in terms of $Q_{UV,T}$ instead of reaction time allows a better comparison due to the change of solar conditions during different experiments.

### 2.3. Analytical methods

The concentration of aqueous cefuroxime was analyzed using liquid chromatography coupled to ultraviolet detection in a UFLC Shimadzu Prominence LC-20AD. A mixture of acetonitrile(A): ultrapure water (B, 0.1% v/v $H_3PO_4$) with an A:B ratio of 20:80 was

pumped at a rate of 0.6 mL $min^{-1}$. The separation was performed in a Kinetex® C18 column (150x4.6 mm, 5µm), whose temperature was maintained at 40 ºC. Quantification was set at 278 nm. The limit of detection and quantification [18] were, respectively, 21.8 and 72.6 µg $L^{-1}$.

Total Organic Carbon (TOC) was determined in a TOC analyzer based on catalytic combustion and non-dispersive infrared detection (Shimadzu®, TOC-$V_{CSH}$), equipped with automatic sample injection. Inorganic anions and short organic acids were analyzed by ion chromatography and conductivity detection in a Metrohm® 881 compact IC pro device with chemical suppression. The column used for separation was a MetroSepA Supp 5 (250x4.0mm, 5µm), kept at 45ºC. A gradient of $Na_2CO_3$ from 0.6mM to 14.6 mM was pumped at 0.7 mL $min^{-1}$ for 60 min.

The concentration of dissolved ozone in the water phase was analyzed by the spectrophotometric method based on indigo trisulfonate decolorization [19].

The initial transformation products during cefuroxime ozonation were identified by liquid chromatography coupled to Quadrupole Time of Flight (LC-QTOF). For the LC separation, an Agilent 1260 HPLC was used whereas the QTOF device was an Agilent 6520 Accurate Mass QTOF LC/MS, equipped with electrospray ionization (ESI). The chromatographic stationary phase consisted of a Zorbax SB-C18 column (3.5 µm, 4.6 × 150 mm) equilibrated at 30 °C. The mobile phase was a mixture of pure Milli-Q® water and acetonitrile. The elution gradient, flow rate 0.4 mL $min^{-1}$, was initially increased from 10% of acetonitrile to 90% in 25 min and kept thereafter for 2 min before equilibration. The QTOF conditions were as follows: ESI(-) mode, gas temperature 325 °C, drying gas 10 mL $min^{-1}$, nebulization 45 psig, Vcap 3500 V, fragmentation 100 V, acquisition m/z range 100–1000. The software Agilent Mass Hunter Qualitative Analysis B.04.00 was used for the interpretation of the results.

## 3. RESULTS AND DISCUSSION

### 3.1. Cefuroxime ozonation kinetics

*3.1.1. Preliminary tests. Stoichometry, elucidation of the kinetic regime and the ozone-CFX reaction rate constant*

Some preliminary tests in the bubble reactor were carried out to study the relative importance of direct, i.e. molecular ozone attack; and indirect, i.e. radical pathway, during ozonation of cefuroxime. The addition of *tert*-butyl alcohol (TBA), is commonly used to suppress the contribution of hydroxyl radical in ozonation tests since the respective second-order rate constants of TBA with ozone and $HO^{\bullet}$ are known: $10^{-3}$ [20] and $6.2 \cdot 10^{8}$ [21] $M^{-1}$ $s^{-1}$, respectively. Fig. 2A shows the temporal evolution of cefuroxime (CFX) during ozonation in the presence and absence of TBA at two different pH values representing acidic (pH~2) and neutral (pH=7) conditions. These two values were considered to check the possible reactivity change of the non-dissociated and dissociated form of CFX (pKa=3.15 [22]). As illustrated in Fig. 2A, higher reactivity at neutral conditions was registered if compared to acidic conditions. Surprisingly, the addition of TBA did not inhibit the reaction rate as expected; on the contrary, it was improved as CFX was completely removed in less time than in the absence of TBA, e.g. at pH=7 CFX was removed in 10 min in absence of TBA and 6 min with TBA 50 mM. This behavior only can be understood if the mass transfer process affects the overall reaction rate and not the reaction by itself. It is well known that the presence of TBA decreases the surface tension of the solution; therefore, hindering the coalescence of the bubbles [23], which affects the mass transfer parameters. Specifically, the interfacial area of the contact between the liquid and gas phase is considerably raised [24,25]; hence, the volumetric ozone mass transfer, $k_La$ increases affecting positively the heterogeneous gas-liquid reaction. This behavior

evidences that the ozonation of CFX is probably limited by the mass transfer process and a high value of the rate constant for the reaction of CFX and $O_3$ must proceed.

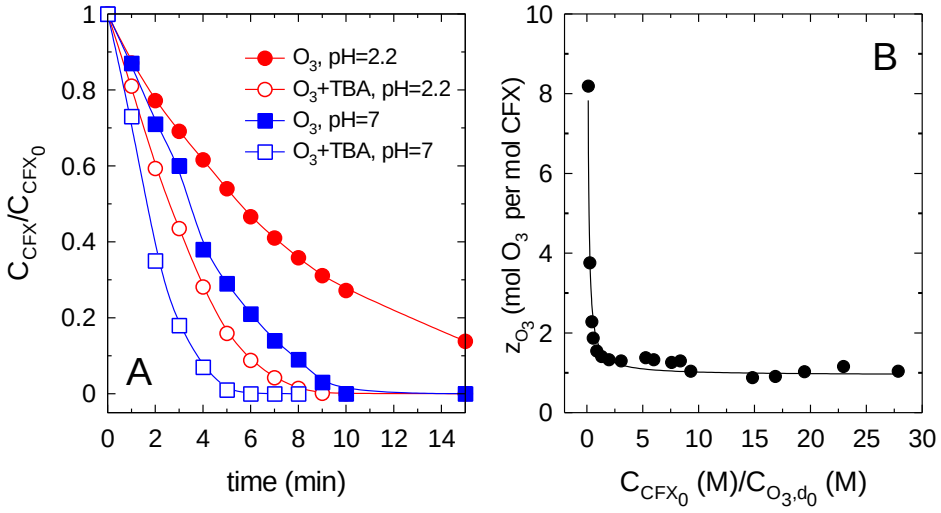


**Figure 2.** Preliminary ozonation tests of cefuroxime. A, Influence of TBA on CFX ozonation in the bubble reactor. Experimental conditions: V=500 mL; $F_{O3,GAS\ inlet}$= 2.2 mg $min^{-1}$; $C_{CFX,0}$=60 mg $L^{-1}$; $C_{TBA}$= 50 mM; pH buffered with $H_3PO_4$ 10 mM. B, Determination of the stoichiometry reaction between $O_3$ and CFX by homogeneous method. Experimental conditions: V= 5 mL; $C_{CFX,0}$=71.2-5.5 mg $L^{-1}$; $C_{O3,d0}$= 5.52-0.30 mg $L^{-1}$; unbuffered pH.

The stoichiometric ratio between the reaction of ozone and CFX was determined in homogeneous reactions in which saturated dissolved ozone was in contact with a known CFX concentration solution. As explained in the experimental section, the representation of $z_{O3}$ *versus* the initial ratio $C_{CFX,0}/C_{O3,0}$ (see Fig. 2B) led to an asymptotic value $z_{O3}$=1.00±0.06 (mol $O_3$ per mol CFX).

*3.1.2. Kinetics study in an agitated-cell reactor*

As deduced from the preliminary tests and the lack of dissolved ozone in the liquid phase, the heterogeneous reaction of CFX ozonation develops in a fast kinetic regime in which the volumetric mass transfer affects the depletion rate of the antibiotic. Moreover, some compounds change their reactivity towards ozone if presented as protonated or

241 deprotonated form [6]. Thus, taking this into account, i.e., $pK_a$=3.15, the quantification
242 of the ozone rate constant ($k_{O3,CFX}$) was tried at pH 2 to 5.

243 To avoid the complex determination of the interfacial area (a) in a bubbled reactor,
244 an agitated cell reactor (Fig. 1A) was used for the estimation of the second-order rate
245 constant of the reaction between molecular $O_3$ and CFX. The agitated cell disposition
246 allows to deduce the volumetric mass transfer, very useful in fast reactions, and
247 accurately calculate the 'a' parameter. In this semi-batch ozonation process, where a
248 non-steady state takes place, the mass balance of CFX in the liquid phase yields to:

249 $$-\frac{dC_{CFX}}{dt} = z_{CFX} N_{O_3} a \quad (4)$$

250 where $N_{O3}$ represents the mass transfer of ozone flux.

251 The application of Fick's law considering the film theory for irreversible second-
252 order reactions allows the absorption rate of $O_3$ to be estimated ($N_{O3}a$, mol $s^{-1}$ $L^{-1}$).
253 This gas-liquid reaction presents a fast kinetic regime and, hence, it develops in the
254 liquid film closed to the gas-water interface. As mentioned above the absence of
255 dissolved ozone confirms the fast kinetic regime of CFX ozonation. Therefore, the $O_3$
256 absorption rate can be defined under these conditions as [15]:

257 $$N_{O3}a = k_L a C^*_{O_3} E = k_L a C^*_{O_3} \frac{Ha'}{\tanh\left(Ha'\right)} = k_L a C^*_{O_3} \frac{Ha_2 \sqrt{\frac{E_i - E}{E_i - 1}}}{\tanh\left(Ha_2 \sqrt{\frac{E_i - E}{E_i - 1}}\right)} \quad (5)$$

258 where $k_La$ is the volumetric mass transfer of $O_3$ in the liquid film, $Ha_2$ is the
259 dimensionless Hatta number for second-order ozone-CFX reaction, E and $E_i$ represent,
260 respectively, the reaction factor and instantaneous reaction factor dimensionless

numbers. It is noteworthy to say that Eq. (5) considers constant concentration of CFX in the reaction liquid film zone as proposed by Van Krevelen and Hoftijzer [26].

Since ozone is a sparingly gas in water, gas resistance to ozone mass transfer is negligible, the concentration of ozone at the interphase can be obtained as follows:

$$C_{O_3}^{*} = \frac{P_{O_3}}{He} = \frac{C_{O_3,g} RT}{He} \tag{6}$$

where He is the Henry's constant for the ozone-water system, R the universal constant of ideal gases, T the absolute temperature and $C_{O3,g}$ the $O_3$ concentration in the gas phase leaving the reactor because of perfect mixing conditions. In this case, however, due to the low ozone absorption rate in the agitated cell reactor, the concentration of ozone in the inlet gas is practically that of the outlet gas. The dimensionless numbers defined before are calculated as:

$$Ha_2 = \frac{\sqrt{D_{O_3} k_{O_3,CFX} C_{CFX}}}{k_L} \tag{7}$$

$$E_i = 1 + \frac{D_{CFX} C_{CFX}}{z_{CFX} D_{O_3} C_{O_3}^{*}} \tag{8}$$

$$E = \frac{N_{O_3} a}{k_L a C_{O_3}^{*}} \tag{9}$$

where $D_{O3}$ (1.40 x $10^{-9}$ $m^2$ $s^{-1}$ [27]) and $D_{CFX}$ (5.52 x $10^{-9}$ $m^2$ $s^{-1}$, estimated with Wilke-Chang empirical formula [28]) are the molecular diffusivities of $O_3$ and CFX in water, respectively; $k_{O3,CFX}$ is the second-order rate constant of the reaction between $O_3$ and CFX and $k_L$ the $O_3$ individual liquid phase mass-transfer coefficient in the agitated cell reactor.

Solution of Eq. 5, due to its complexity, implies a trial and error procedure in which $k_{O3,CFX,}$ and $k_L$ are unknown. For that reason, two simplified fast kinetic subregimes, depending on the $Ha_2$ value, were considered.

*Fast pseudo-first-order kinetic regime ($3 \leq Ha_2 \leq E_i/2$)*

This regime supposes that the concentration of CFX is constant in all liquid zone (that is, in both liquid film and bulb) and the reaction zone develops in the liquid film. In that case, and if the condition $3 \leq Ha_2 \leq E_i/2$ holds, the reaction factor and Hatta numbers coincide ($E=Ha_2$). Then, the CFX balance in the semi-batch reactor yields [12]:

$$-\frac{dC_{CFX}}{dt} = z_{CFX} k_L a C_{O_3}^* Ha_2 = z_{CFX} a C_{O_3}^* \sqrt{D_{O_3} k_{O_3,CFX} C_{CFX}} \qquad (10)$$

which after integration, considering $C_{O_3}^*$ calculation through Eq. 6 and constant with time in the agitated cell reactor, leads to:

$$2\left(\sqrt{C_{CFX_0}} - \sqrt{C_{CFX}}\right) = z_{CFX} a \frac{C_{O_3,GAS} RT}{He} \sqrt{D_{O_3} k_{O_3,CFX}}\, t \qquad (11)$$

The linear representation of the left side of the previous equation *versus* time conducts to a straight line that after least squares analysis $k_{O3,CFX}$ can be calculated from the slope of the line. Fig. 3A depicts the validation of Eq. 11 for ozonation tests in the agitated cell reactor at different pH values in the range 2-5. Table 2 shows the calculated second-order rate constant obtained after linear regression. However, to validate that $3 \leq Ha_2 \leq E_i/2$, the value of the $O_3$ individual liquid phase mass-transfer coefficient is required. For that purpose, experiments of ozone absorption-decomposition in the absence of CFX were carried out in the agitated cell reactor and the dissolved ozone in the liquid phase was monitored. Thus, the liquid phase was saturated with ozone, and then after

interrupting ozone feeding, the decomposition of dissolved ozone was followed. The rate of absorption and decomposition can be described by the respective equations:

*Absorption period:* $$\frac{dC_{O_3}}{dt} = (k_L a + k_1)\left(C_{O_3,s} - C_{O_3}\right) \quad (12)$$

*Saturation period:* $$C_{O_3} = C_{O_3,s} \quad (13)$$

*Decomposition period:* $$-\frac{dC_{O_3}}{dt} = k_1 C_{O_3} \quad (14)$$

where $C_{O3,s}$ means the dissolved ozone concentration at the gas-liquid interface or solubility . Fig. 3B depicts the evolution of dissolved $O_3$ in the aforementioned experiment of $O_3$ absorption-decomposition. The different slopes between the two regions led to $k_1=(1.4\pm0.1)\cdot10^{-4}$ $s^{-1}$ and $k_L=(1.1 \pm 0.1)\cdot10^{-5}$ m $s^{-1}$. Known $k_L$, $Ha_2$ and $E_i$ numbers can be calculated to validate the kinetic regime initially supposed. Table 2 shows results for each pH situation. Since both dimensionless numbers are a function of time, the range of these values in the interval of reaction studied (initial, $t_0$; and after 60 min, $t_{60}$) are calculated.

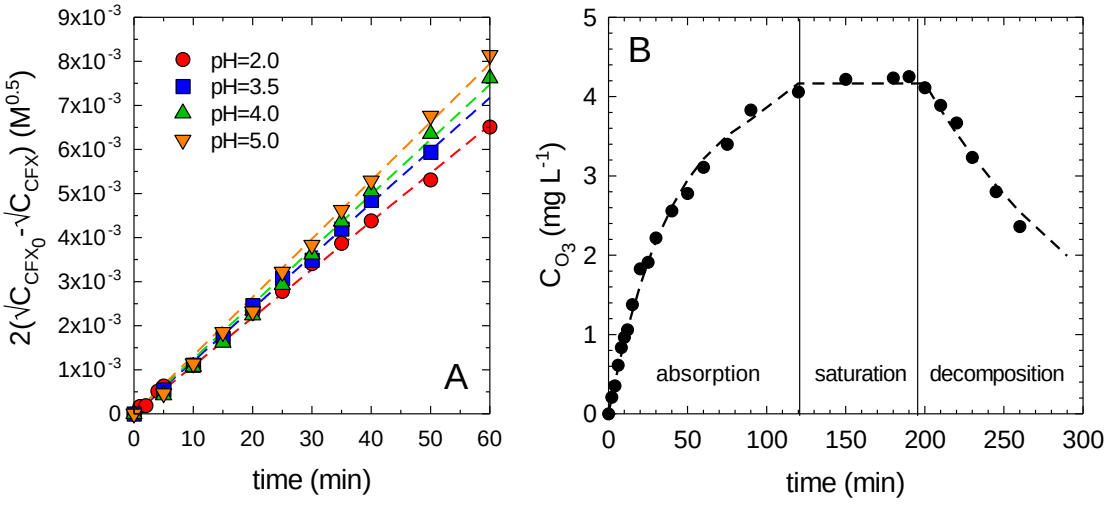


**Figure 3.** Cefuroxime ozonation in the agitated cell reactor. A, Experimental fitting to the fast pseudo-first regime, validation of Eq. 11. Experimental conditions: V=500 mL; $C_{CFX,0}$ =70 mg $L^{-1}$; $C_{O3,GAS}$ inlet=4.0 mg $L^{-1}$; $C_{TBA}$= 50 mM; buffered pH with $H_3PO_4$ 10

mM. B, Determination of $k_L$ coefficient in the absence of cefuroxime. Experimental conditions: V=500 mL; $C_{O3,GAS}$ inlet=50 mg $L^{-1}$; pH=2.0 (buffered with $H_3PO_4$ 10 mM). Dashed lines: modeling with the respective equations.

**Table 2.** Application of fast pseudo-first order kinetic regime to the cefuroxime ozonation. Parameters obtained from fitting experimental data to Eq. 11.

| pH | $R^2$ | $k_{O3,CFX}$ ($M^{-1}$ $s^{-1}$) | $Ha_2$ | | $E_i$ | |
|---|---|---|---|---|---|---|
| | | | $t_0$ | $t_{60}$ | $t_0$ | $t_{60}$ |
| 2.0 | 0.994 | $(4.6\pm0.2)\cdot10^6$ | 112 | 84 | 3.6 | 2.4 |
| 3.5 | 0.998 | $(6.8\pm0.2)\cdot10^6$ | 129 | 73 | 3.6 | 1.8 |
| 4.0 | 0.996 | $(8.7\pm0.3)\cdot10^6$ | 124 | 72 | 3.0 | 1.7 |
| 5.0 | 0.997 | $(1.12\pm0.03)\cdot10^7$ | 167 | 103 | 4.1 | 2.2 |

According to results shown in Table 2 the condition of fast pseudo first kinetic regime of ozone-CFX reaction ($3\leq Ha_2\leq E_i/2$) is not fulfilled. Then, rate constant values obtained cannot be taken as definitive though likely on the order of magnitude of the actual ones.

*Instantaneous kinetic regime ($Ha_2>>10E_i$)*

The fast instantaneous kinetic regime is characterized by a rate controlled exclusively by the diffusion rate of reactants, $O_3$, and the antibiotic, through the liquid film. As indicated above, the gas phase does not present any resistance to $O_3$ diffusion due to its low solubility in water. Under these conditions, the reaction develops in a plane inside the film layer close to the gas-water interface and the reaction factor is defined by the instantaneous reaction factor number ($E=E_i$) [29]:

$$-\frac{dC_{CFX}}{dt} = z_{CFX}\,k_L a C^*_{O_3} E_i = z_{CFX}\,k_L a C^*_{O_3}\left(1+\frac{D_{CFX}\,C_{CFX}}{z_{CFX}\,D_{O_3}\,C^*_{O_3}}\right) \qquad (15)$$

This equation holds for compounds that present a high reaction rate constant towards ozone, so that $Ha_2>>10E_i$ holds. The integration of Eq. 15 for a given time, t, yields to:

$$\ln(\vartheta) = \frac{k_L a D_{CFX}}{D_{O_3}} t \quad (16)$$

where the parameter $\vartheta$ means:

$$\vartheta = \frac{C_{CFX_0} + \frac{z_{CFX} D_{O_3} C^*_{O_3}}{D_{CFX}}}{C_{CFX} + \frac{z_{CFX} D_{O_3} C^*_{O_3}}{D_{CFX}}} \quad (17)$$

The representation of $\ln(\vartheta)$ *versus* time at each pH value generates a straight line from whose slope $k_L$ can be obtained. Fig. 4A shows the representation of Eq. 17 and Table 3 the obtained $k_L$ values. However, the second-order rate constant values cannot be experimentally determined under these conditions since the process is controlled by $O_3$ and CFX mass transfer. Nevertheless, a minimum value for $k_{O3,CFX}$ that holds the condition $Ha_2 >> 10E_i$ can be calculated:

$$E_i = \frac{1}{10}(Ha_2)_{\min} \quad (18)$$

$$E_i = \frac{1}{10} \frac{\sqrt{D_{O_3}(k_{O_3,CFX})_{\min}}}{k_L} \sqrt{C_{CFX}} \quad (19)$$

The fitting of the $E_i$ dimensionless values *versus* $\sqrt{C_{CFX}}$ during the reaction course allows the determination of a minimum value for the second-order rate constant of the ozonation reaction, $(k_{O3,CFX})_{min}$, see Fig. 4B.

**Table 3.** Application of the fast instantaneous kinetic regime to the cefuroxime-ozone reaction. Parameters obtained from fitting experimental data to Eqs. 16 and 19.

| pH | From Eq. 16 | | From Eq. 19 | |
|---|---|---|---|---|
| | $R^2$ | $k_L$ (m $s^{-1}$) | $R^2$ | $(k_{O3,CFX})_{min}$ ($M^{-1}$ $s^{-1}$) |
| 2.0 | 0.997 | $(1.68\pm0.06)\cdot10^{-5}$ | 0.9995 | $(1.18\pm0.02)\cdot10^{6}$ |
| 3.5 | 0.998 | $(1.95\pm0.06)\cdot10^{-5}$ | 0.9994 | $(1.81\pm0.02)\cdot10^{6}$ |

| | | | | |
|---|---|---|---|---|
| 4.0 | 0.996 | $(2.19\pm0.08)\cdot10^{-5}$ | 0.9991 | $(1.92\pm0.02)\cdot10^{6}$ |
| 5.0 | 0.994 | $(2.30\pm0.10)\cdot10^{-5}$ | 0.9993 | $(3.51\pm0.03)\cdot10^{6}$ |

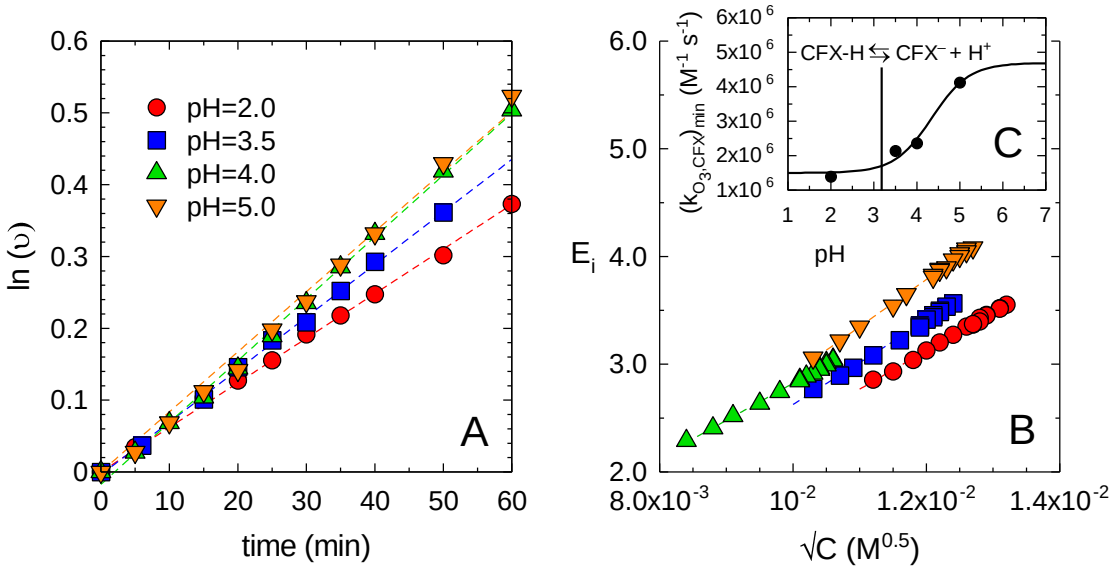


**Figure 4.** Cefuroxime ozonation in the agitated cell reactor. A, Experimental fitting to the fast instantaneous regime, validation of Eq. 17. B, Determination of $(k_{O3,CFX})_{min}$, validation of Eq. 19. C, Influence of pH on the second-order rate constant. Experimental conditions as shown in Fig. 3.

The calculated values of the minimum second-order rate constant show a slight increase with a rise of pH due to the acid character of cefuroxime (pKa=3.15). This fluctuation does not affect the kinetic regime in which the process holds and it is a different response, but still similar, to the acid-base CFX dissociation. Accordingly, the values for the non-dissociated and dissociated forms were estimated through the expressions:

$$(k_{O_3,CFX})_{\min} = (1-\alpha)(k_{O_3,neutral})_{\min} + \alpha(k_{O_3,dissociated})_{\min} \quad (20)$$

$$\alpha = \frac{1}{1+10^{pK_a-pH}} \quad (21)$$

where α is de dissociation degree, $(k_{O3,neutral})_{min}$ and $(k_{O3,dissociated})_{min}$ are, respectively, the minimum values of the second-order rate constant with the non-dissociated and dissociated species of CFX. Eq. 20 was fitted to experimental data, leading to these two

respective values for the ozone reactions with non-dissociated and dissociated CFX species: $1.50 \times 10^6$ and $4.69 \times 10^6$ $M^{-1}$ $s^{-1}$.

### *3.1.3. Identification of first oxidation intermediates*

The first oxidation intermediates during cefuroxime oxidation were identified by LC-QTOF in the agitated cell reactor. Experiments were carried out in the cell agitated reactor under the same experimental conditions of the previous kinetic study and five transformation products were registered. The monoisotopic mass M=442.40 corresponds to the hydroxylation of CFX molecule. *In silico* tools that predict the oxidation pathway of this molecule, such as Pathway Prediction System and PathPred [30], include the hydroxylation onto the unsaturated double bond of the non-aromatic ring. However, this oxidation can also take place in the furan aromatic ring, as proposed in Fig. 5. The N of the secondary amide group acting as a bridge is a potential breakable point of CFX molecule by ozone attack as deduced from the observed intermediates. Two different fragmentation patterns can be displayed depending on what part maintains the $–NH_2$ group. The first break pattern involves the formation of an unsubstituted amide group and a ketone in the ring of four atoms (M=272.23). This breakage should also give rise to the formation of the unsubstituted amide containing the furan ring; however, this intermediate (M=168.05) was not detected. Further oxidation of M=272.23 product onto S heteroatom lead to the rupture of the substituted sulfide-containing ring and the formation of product M=272.17. The oxidation of the alcohol group into aldehyde triggers the formation of M=270.15. The second route for the rupture of the secondary amide group of CFX leads to the formation of a carboxylate (M= 169.04) and an unsubstituted amine (M=273.04), as Fig. 5 shows. Neither of them was detected, probably due to a high reactivity in such an oxidative

medium. Nevertheless, the oxidation of the non-detected amine onto the substituted sulfide atom led to the corresponding sulfoxide, monoisotopic mass M=266.26.

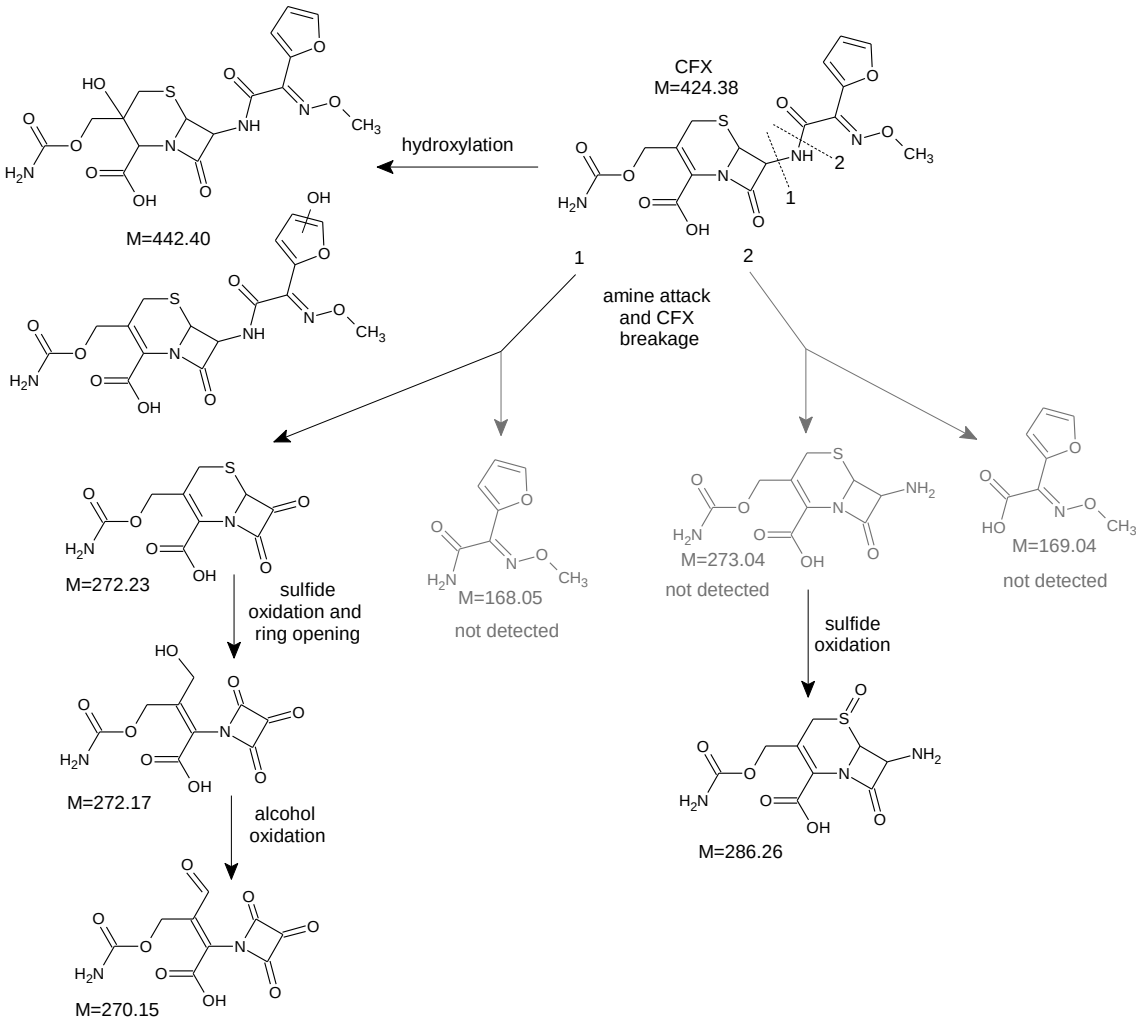


**Figure 5.** Identified intermediates during ozone oxidation of cefuroxime (CFX) and the tentative oxidation pathway

### 3.2. Photo-assisted ozonation of cefuroxime in solar CPC reactors

Degradation of cefuroxime was further studied in a solar CPC reactor. Firstly, experiments in ultrapure water were achieved. The photolysis of CFX by solar radiation led to a slow degradation as shown in Fig. 6A. According to the CFX UV-visible absorption spectrum, CFX is expected to be activated with radiation below 330 nm, see Fig. 6C. The solar radiation wavelength reaching the solid after the glass cutoff of the pipe was over 300 nm. Therefore, the proportion within 300-330 nm is responsible for

406 the photolytic activation of CFX. On the contrary of the pseudo-first order kinetics
407 usually observed in photolytic activation, a 40% of CFX degradation is registered in the
408 first 30 min, followed by a pseudo-first order depletion afterward (pseudo-observed rate
409 constant, 0.148±0.009 $h^{-1}$).

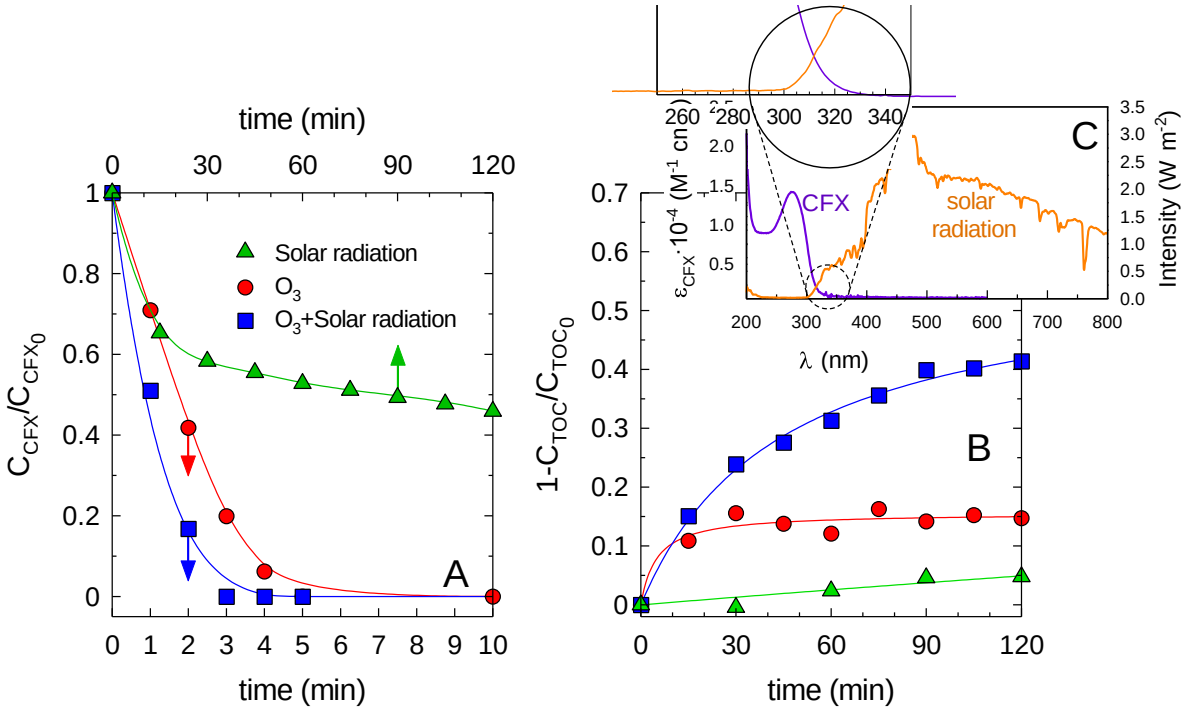


410

411 **Figure 6.** Cefuroxime removal in ultrapure water by solar photo-assisted ozonation in
412 the CPC reactor. A, Normalized evolution of CFX concentration with time. B,
413 mineralization evolution. C, Extinction molar coefficient of CFX ($\varepsilon_{CFX}$) and intensity of
414 the solar radiation spectrum. Experimental conditions: V=5.0 L; $C_{CFX,0}$ =12.8±0.4 mg
415 $L^{-1}$; $C_{TOC,0}$=5.8±0.2 mg $L^{-1}$; $Q_{GAS}$=30 L $h^{-1}$; $C_{O3,inlet}$=17 mg $L^{-1}$; $pH_i$=5.2±0.4
416 (unbuffered); $pH_f$=4.75±0.1.

417 The removal rate of CFX was considerably improved in the presence of ozone, due to
418 the high reactivity of this molecule towards ozone. For comparison purposes, single
419 ozonation in the CPC installation was conducted in the dark. As depicted in Fig. 6A, the
420 application of only ozone was capable of oxidizing all the CFX in 10 min under the
421 conditions applied. The addition of solar radiation led to an acceleration of the oxidation
422 rate as CFX was completely removed in less time, 3 min. As a mere comparison tool,

423 the pseudo-first order rate constant of the three processes is calculated in time and
424 absorbed energy units:

425 $$-\frac{dC_{CFX}}{dt} = kC_{CFX} \quad or \quad -\frac{dC_{CFX}}{dQ_{UV}} = kC_{CFX} \tag{22}$$

426 If irradiated systems are compared, photolytic ozonation (SR-$O_3$) and photolysis (SR,
427 second decay after 30 first minutes) led to respective k values, $k_{SR}$=1.08±0.05 $kJ^{-1}$ L or
428 0.148±0.009 $h^{-1}$ and $k_{SR-O3}$=658±38±0.05 $kJ^{-1}$ L or 70±3 $h^{-1}$. As single ozonation was
429 conducted in the dark, only the temporal pseudo-first order constant can be calculated.
430 The application of ozone led to a value of $k_{O3}$=43±2 $h^{-1}$. The application of $O_3$ exerts
431 much faster oxidation than solar photolysis, and the join of these two improves the
432 results. Only 38% of synergism percentage calculated as $[k_{SR-O3}-(k_{SR}+k_{O3})]/k_{SR-O3}$ is
433 registered.

434 The ozone consumption is a better parameter to understand how ozone uptake is
435 harvested in both systems instead of time units. The ozone consumption was determined
436 as the transferred ozone dose (TOD) which represents the accumulated amount of ozone
437 that is consumed by the aqueous solution in a given time, t [31]:

438 $$TOD = \int_0^t \frac{Q_{GAS}}{V}\left(C_{O_3,g,inlet} - C_{O_3,g,outlet}\right) dt \tag{23}$$

439 where $Q_{GAS}$ stands for the gas flow rate, V the liquid volume, $C_{O3,g,inlet}$ and $C_{O3,g,out}$ the
440 ozone concentration entering and leaving the reactor, respectively. The results are
441 shown in the Fig. 6. The Fig. 6A shows a lower ozone consumption. For a complete
442 removal of CFX only 1 mg $O_3$ $L^{-1}$ was consumed if solar radiation was accomplished to
443 ozonation. Single ozonation required a larger $O_3$ dose, i.e. 8.6 mg $O_3$ $L^{-1}$. These
444 facts confirms the enhanced effect of radiation that promotes the oxidation of CFX
445 by the indirect pathway of ozonation, that means the formation of powerful
radicals, $HO^{\bullet}$

446 mainly, that present higher reactivity (second order rate constant $k_{CFX,\ HO^{\bullet}}$=1.2 x $10^{10}$
447 $M^{-1}$ $s^{-1}$ [32]).

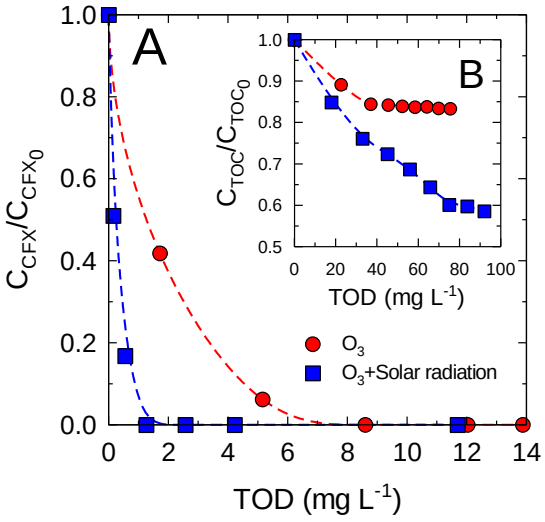


448

449 **Figure 6.** Cefuroxime removal in ultrapure water by solar photo-assisted ozonation
450 in the CPC reactor as a function of the Transferred Ozone Dose (TOD). Cefuroxime
451 (A) and mineralization (B) evolution as a function of TOD. Experimental
452 conditions as shown in the Fig. 6.

453 The kinetics in the photo-reactor was simulated by determining the partial
454 contributions of the individual processes, i.e. photolysis and ozonation. Firstly, the
455 kinetics of the photolysis of cefuroxime can be described by the following expression
456 based on the Lambert-Beer law [33]:

457 $$r_{CFX,SR} = -\frac{dC_{CFX}}{dt} = \phi_{CFX} I_0 \frac{\varepsilon_{CFX} C_{CFX}}{\Sigma \varepsilon_i C_i}\left(1 - e^{-2.303 L \Sigma \varepsilon_i C_i}\right) \quad (24)$$

458 where $\phi_{CFX}$ is the photochemical reaction quantum yield, $\varepsilon_{CFX}$ the extinction coefficient,
459 $I_0$ the incident radiation on the CPC glass tubes, $C_i$ the concentration of the radiation
460 absorbing species, and L the effective path of radiation in the photo-reactor (21% of the
461 inner diameter of the CPC pipe [34]). Assuming that the main absorbance substance is
462 the parent compound, i.e. CFX, then . The previous $\Sigma \varepsilon_i C_i \approx \varepsilon_{CFX} C_{CFX}$ assumption is based

463 on the fact that intermediates are generated in a smaller concentration than CFX. Taking
464 into account an average value for $\varepsilon_{CFX}$ (2382 $M^{-1}$ $cm^{-1}$) and $I_0$ (4.06 $10^{-5}$ Einstein L
465 $s^{-1}$) within the range 320-337 nm , the eq. (24) can be analytically solved to give [35]:

466 $$C_{CFX_0} - C_{CFX} + \frac{1}{\alpha}\ln\left(\frac{1-e^{-\alpha C_{CFX_0}}}{1-e^{-\alpha C_{CFX}}}\right) = \phi_{CFX} I_0 t \qquad (25)$$

467 where $\alpha = 2.303 L \varepsilon_{CFX}$ . From the fitting of experimental data to eq. (25), the average
468 value within 320-337 nm of the quantum yield for CFX was found to be $\phi_{CFX}$=1.44 $10^{-4}$
469 mol $Einstein^{-1}$. No reported values in the literature for CFX are available. Nevertheless,
470 this value is lower than other average quantum yields reported for
471 cephalosporin antibiotics [36] under solar radiation using the whole solar spectrum
472 (295-800 nm). It must be considered that the cut-off of the glass tubes of the photo-
473 reactor limits the radiation absorption to 320-337 nm and this aspect is likely the
474 reason of a lower quantum yield calculated in this work.

475 Secondly, the Eq. (15) for the ozonation in the fast instantaneous kinetic regime was
476 used to fit the experimental data of ozonation in the CPC photo-reactor. Then, the
477 volumetric mass transfer coefficient, $k_La$, was estimated by fitting the Eq. (15) to
478 the ozone experimental results. Since the reaction between ozone and CFX is
479 instantaneous, hydroxyl radical contribution to remove CFX was assumed negligible.
480 Accordingly, the $k_La$ was found to be 1.37 x $10^{-3}$ $s^{-1}$.

481 The CFX removal rate by solar photolytic ozonation ($r_{CFX,SR+O3}$) can be
482 expressed according to the Eq. (26) in which photolysis ($r_{CFX,SR}$), ozone ($r_{CFX,O3}$)
483 and hydroxyl radical ($r_{CFX,HO\bullet}$) contributions are considered:

484 $$r_{CFX,SR+O_3} = r_{CFX,SR} + r_{CFX,O_3} + r_{CFX,HO\bullet} \qquad (26)$$

485 with the hydroxyl radical contribution rate given by the Eq. (27):

$$r_{CFX,HO^{\bullet}} = k_{CFX,HO^{\bullet}} . C_{HO^{\bullet}} . C_{CFX} \quad (27)$$

where $k_{CFX,HO^{\bullet}}$ and $C_{HO^{\bullet}}$ are the rate constant of the CFX-HO reaction and the concentration of hydroxyl radicals, respectively. The degradation rate of CFX by photolytic ozonation ($r_{CFX,SR+O3}$) was calculated from the experimental data. The Eqs. (25) and (15) were used for the estimation of the contribution of photolysis and ozonation, respectively. Considering the second-order rate constant for $HO^{\bullet}$ reaction, $k_{CFX,\ HO^{\bullet}}$=1.2 x $10^{10}$ $M^{-1}$ $s^{-1}$ [32], the steady state concentration of $HO^{\bullet}$ was obtained, $C_{HO^{\bullet}}$=3.90 x $10^{-14}$ M. Moreover, the relative importance of hydroxyl radical was confirmed by calculating the overall ratio of this contribution, $r_{CFX,HO^{\bullet}}$/ $r_{CFX,SR+O3}$=55%. Over a half of the kinetic contribution of CFX removal was due to hydroxyl radical action.

Greater differences are appreciated in terms of mineralization, see the Fig. 6B. Photolytic ozonation was capable of achieving approximately 40% of TOC removal after 2 h reaction whereas in the absence of radiation ozone only led to 15% of mineralization. It is noteworthy to say, that ozonation mineralization degree was inhibited since the first 15 min while the addition of radiation to the ozonation system conducted to a gradual increase of mineralization percentage due to the ability of UVA radiation to enhance the ozone decomposition in water for producing hydroxyl radical in a greater extent [13]. The better use of the consumed ozone is also appreciated when analyzing the evolution of TOC removed as a function of TOD. The simultaneous application of ozone and solar radiation led to a 41% mineralization with a TOD=80 mg $O_3$ $L^{-1}$ whereas single ozonation only led a 17% of mineralization under the same TOD. This difference is undoubtedly due to the larger amount of $HO^{\bullet}$ generated that increases the TOC removal rate. Further analysis of the nature of the remaining TOC was carried out by monitoring the release of short organic acids. Acetic, formic, pyruvic, and oxalic

511 acids were mainly detected during the oxidation of CFX. As shown in Fig. 7, the major
512 differences account for acetic acid. Photo-ozonation produces a higher amount of acetic
513 acid than the application of ozone alone (~5 *vs* 2.7 mg $L^{-1}$). Moreover, the release of the
514 organic nitrate from CFX molecule (4 N atoms per molecule) was complete after 90 min
515 with the joint application of radiation and ozone. In the absence of solar radiation, after
516 120 min of treatment, still, an extra 12% of nitrate was expected to be released. If
517 profiles of nitrate and acetic acid during ozonation are analyzed, it is observed that, due
518 to their temporal evolution, the release trends of nitrate and acetic acid are similar. The
519 rest of the organic acids, formic, pyruvic, and oxalic, are generated, approximately, at
520 the same extent in both processes. However, the solar photo-ozonation achieves a
521 maximum acid concentration in the first 15 min followed by a slow decrease afterward.
522 The temporal evolution of the percentage of the detected organic acids accounting for
523 the TOC ($AO_{TOC}$) indicates a final 42% for photo-ozonation and 27% in ozonation. In
524 the case of photo-ozonation, that means that more organic acids without N in their
525 structure are still present in the solution. In the case of single ozonation, besides,
526 nitrogenized organic species are still present in the solution. The evolution of the sulfate
527 released also shows differences between single ozonation and photolytic ozonation, (see
528 Fig. 7). CFX molecule contains one S atom as heteroatom in a ring that is susceptible to
529 oxidation as previously suggested from the identification of first oxidation products.
530 Over 96% of S contained in the CFX molecule was transformed into sulfate with
531 combined ozone and solar radiation whereas with single ozonation barely reached 54%.
532 This is another extra evidence of lesser mineralization ability of single ozonation
533 application. The addition of radiation results beneficial to increase mineralization and
534 release inorganic species in their highest oxidation state, i.e. nitrogen as nitrate and
535 sulfur as sulfate.

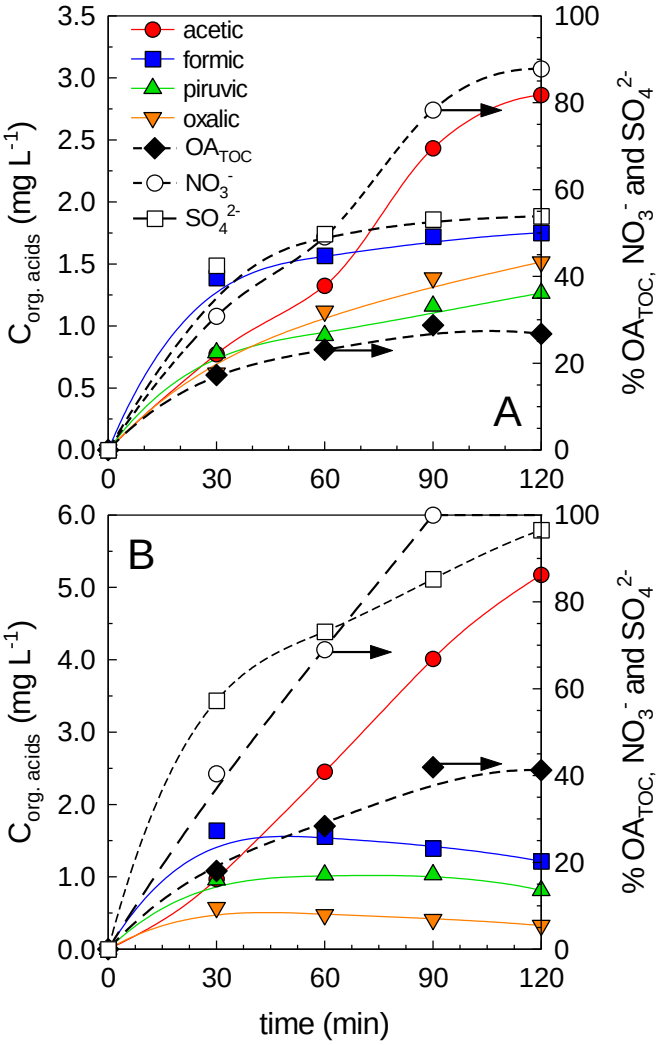


**Figure 7.** Cefuroxime removal in ultrapure water by solar photo-assisted ozonation in the CPC reactor. Evolution of short organic acids (OA), percentage of OA accounting in TOC ($OA_{TOC}$), and percentage of nitrate released during (A) single ozonation and (B) solar photolytic ozonation. Experimental conditions as shown in Fig. 6.

The removal efficiency of CFX was further assessed in a Simulated Urban WasteWater matrix (SUWW, see characterization in Table 1) with a lower concentration of CFX, i.e. 1 mg $L^{-1}$. From Fig. 8A, less difference between ozonation and photolytic ozonation can be appreciated if compared to previous tests in ultrapure water during the evolution of the remaining concentration of CFX, completely removed in 10 min. Different plausible explanations may contribute to the description of this less efficient behavior in the SUWW matrix. The competition for the absorption of light by

548 the Dissolved Organic Matter (DOM) present in the SUWW may lead to a less efficient
549 decomposition of $O_3$ into radicals; or the competition of CFX and DOM or inorganic
550 carbon for the extra reactive species, i.e. hydroxyl radical, generated during photolytic
551 ozonation are the most common reasons. Comparing the pseudo-first order rate
552 constants, photolysis (SR) and photolytic ozonation (SR-$O_3$) led to respective k values,
553 $k_{SR}$=2.1±0.1 $kJ^{-1}$ L or 0.37±0.07 $h^{-1}$ and $k_{SR\text{-}O3}$=137±11 $kJ^{-1}$ L or 28±32 $h^{-1}$. As single
554 ozonation was conducted in the dark, only the temporal pseudo-first order constant can
555 be calculated. The application of ozone led to a value of $k_{O3}$=23±1 $h^{-1}$. The little
556 difference (23 *vs.* 28 $h^{-1}$) of the pseudo rate constants decreases the
557 synergism percentage if compared to the ultrapure water scenario, 10% (SUWW)
558 *vs.* 38% (UP water). In terms of TOD, the comparison of single ozonation and photo-
559 ozonation led to less differences in SUWW matrix if compared to ultrapure water, as
560 shown in the Fig. 9.

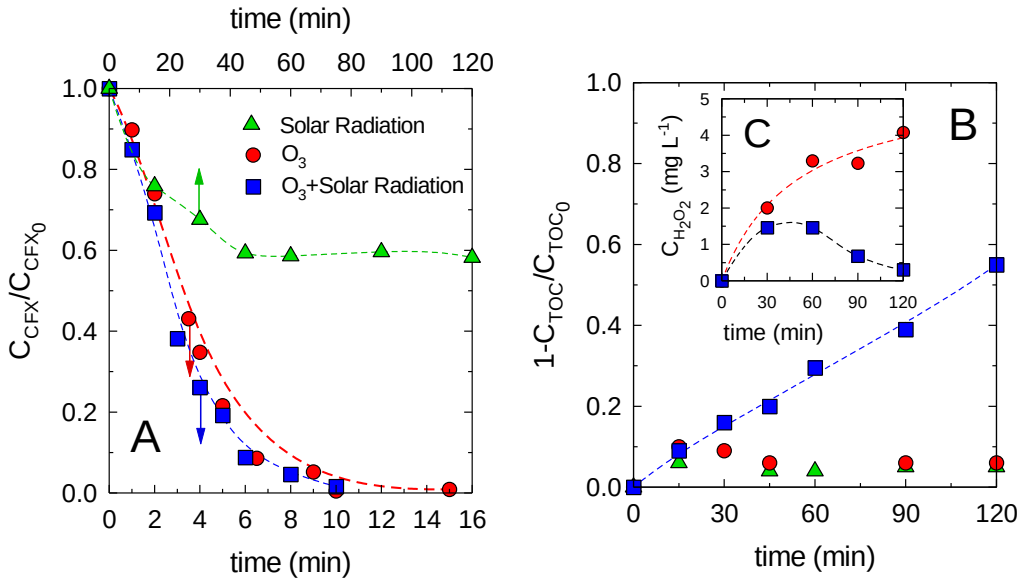


561

562 **Figure 8.** Cefuroxime removal in SUWW by solar photo-assisted ozonation in the CPC
563 reactor. A, Normalized evolution of CFX concentration with time; B, mineralization
564 evolution. C, temporal evolution of released $H_2O_2$. Experimental conditions: V=5.0 L;
565 $C_{CFX,0}$ =1.4±0.4 mg $L^{-1}$; $C_{TOC,0}$=16.6±2.0 mg $L^{-1}$; $Q_{GAS}$=30 L $h^{-1}$; $C_{O3,inlet}$=17 mg $L^{-1}$;
566 $pH_i$=7.0±0.5.

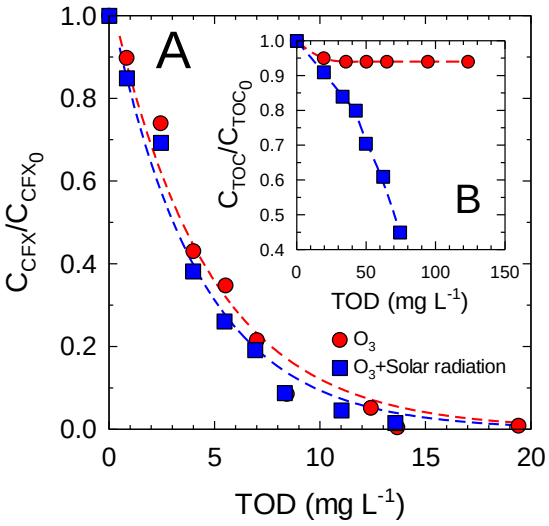


**Figure 9.** Cefuroxime removal in SUWW by solar photo-assisted ozonation in the CPC reactor as a function of the Transferred Ozone Dose (TOD). Cefuroxime (A) and mineralization (B) evolution as a function of TOD. Experimental conditions as shown in Fig. 8.

Significant differences were appreciated by monitoring TOC evolution in both systems. The photolytic ozonation process led to 55% of mineralization in 2 hours whereas single ozonation resulted in negligible oxidation of the organic matter present in the SUWW matrix. The Fig. 10 shows the temporal evolution of global TOC and the accounting amount of short organic acids, i.e. formic, acetic, and oxalic. It is observed that photolytic ozonation results more effective to transform the organic content of the SUWW matrix mainly given the fact that contribution of CFX oxidation to this content is practically negligible, e.g. initial CFX concentration of 1 mg $L^{-1}$. Single ozonation displayed the ability to partially oxidize DOM into the mentioned organic acids due to the low reactivity of ozone molecule towards these molecules [37] and the low potential of single ozonation to produce hydroxyl radicals. However, the addition of solar radiation triggers an effective decomposition of ozone molecule into hydroxyl radicals which explains the higher mineralization degree registered. Regarding comparison of the mineralization evolution versus the TOD, (see the Fig. 9), a more efficient

586 consumption of the ozone transferred in thephotolytic ozonation process is observed
587 with 55% of mineralization and a ~75 mg $O_3$ $L^{-1}$ TOD.

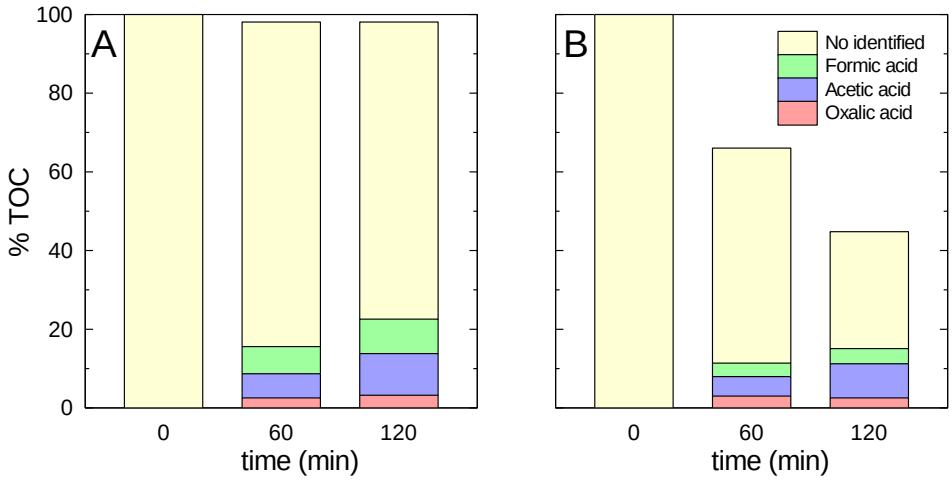


588

589 **Figure 10.** Cefuroxime removal in SUWW by (A) ozonation and (B) solar photo-
590 assisted ozonation in the CPC reactor. Evolution of TOC fractions.
591 Experimental conditions as shown in Fig. 8.

592 The formation of $H_2O_2$ is well known in ozone-based processes. Ozone can be
593 generated during ozone photolysis [11,13] and more importantly during the ozone
594 attack to organic molecules containing unsaturated groups or aromatic rings [38]. The
595 ozonation of DOM present in the SUWW led to a gradual $H_2O_2$ release reaching a
596 maximum concentration of *ca.* 4 mg $L^{-1}$. However, when solar radiation was added, the
597 released $H_2O_2$ profile followed a maximum (around 1.5 mg $L^{-1}$) to almost been
598 completely removed after 2 h (see Fig. 8C). The UV component of solar
599 radiation, especially at wavelength below 360 nm [39], contributes to the
600 photolysis of $H_2O_2$ which supposes an additional source of $HO^{\bullet}$ formation and explains
601 the decay observed during photolytic ozonation.

## CONCLUSIONS

Cefuroxime is a molecule with a high reactivity towards the ozone molecule. The stoichiometric ozonation ratio was estimated as $z_{O3}$=1.00 ± 0.06 (mol $O_3$ per mol cefuroxime) and the second-order rate constant in the range 1.50 x $10^6$ – 4.69 x $10^6$ $M^{-1}$ $s^{-1}$ for the non-dissociated and dissociated, respectively, cefuroxime molecule. Under the operating conditions applied in this study, the ozone absorption rate followed the fast instantaneous kinetic regime. The rate of the ozonation process was exclusively controlled by the diffusion rate of reactants, ozone and the antibiotic, through the liquid film and the reaction develops inside the film layer close to the gas-water interface. The intermediates detected included hydroxylation of the initial molecule, rupture of amide bridge, and oxidation of the bi-substituted sulfide.

Photolytic ozonation is a feasible technology to address the removal of target microcontaminants as cefuroxime in the wastewater matrix by photo-ozonation in a solar pilot plant by the sole action of solar radiation either for irradiating the solar collector reactor and supplying energy requirements of the plant. Therefore, solar radiation could be use not only to enhance ozonation effects but also for electrical energy requirements, maintenance costs would be highly reduced and the increase of mineralization would be useful to treated wastewater for reuse purposes. The simultaneous application of ozone resulted positive to enhance the removal of cefuroxime, just partially due to the high reactivity of cefuroxime towards molecular ozone. However, the mineralization extent was considerably high for the hybrid technology (55% in wastewater matrix). The higher release of sulfate and faster of nitrate also supported the higher mineralization power of the photo-ozonation system. Single ozonation presented a low mineralization ability in ultrapure water (15%), but it

was completely inefficient in the wastewater matrix in which only partial oxidation to accumulated short organic acids was monitored.

**Acknowledgments**

The authors are grateful to Junta de Extremadura (Project IB16022), co-financed by the European Funds for Regional Development, for economically supporting this work.

**References**

[1] M. Pazda, J. Kumirska, P. Stepnowski, E. Mulkiewicz, Antibiotic resistance genes identified in wastewater treatment plant systems – A review, Sci. Total Environ. 697 (2019) 134023. doi:10.1016/j.scitotenv.2019.134023.

[2] J. Rossmann, S. Schubert, R. Gurke, R. Oertel, W. Kirch, Simultaneous determination of most prescribed antibiotics in multiple urban wastewater by SPE-LC-MS/MS, J. Chromatogr. B Anal. Technol. Biomed. Life Sci. 969 (2014) 162–170. doi:10.1016/j.jchromb.2014.08.008.

[3] N. Das, J. Madhavan, A. Selvi, D. Das, An overview of cephalosporin antibiotics as emerging contaminants: a serious environmental concern, 3 Biotech. 9 (2019). doi:10.1007/s13205-019-1766-9.

[4] K. Kümmerer, D.D. Dionysiou, O. Olsson, D. Fatta-Kassinos, A path to clean water, Science. 361 (2018) 222–224. doi:10.1126/science.aau2405.

[5] U. von Gunten, The basics of oxidants in water treatment. Part B: Ozone reactions, in: Water Sci. Technol., 2007: pp. 25–29. doi:10.2166/wst.2007.382.

[6] F.J. Beltrán, A. Rey, Free Radical and Direct Ozone Reaction Competition to Remove Priority and Pharmaceutical Water Contaminants with Single and Hydrogen Peroxide Ozonation Systems, Ozone Sci. Eng. 40 (2018) 251–265. doi:10.1080/01919512.2018.1431521.

[7] D. Daumont, J. Brion, J. Charbonnier, J. Malicet, Ozone UV spectroscopy I: Absorption cross-sections at room temperature, J. Atmos. Chem. 15 (1992) 145–155. doi:10.1007/BF00053756.

[8] J. Brion, A. Chakir, J. Charbonnier, D. Daumont, C. Parisse, J. Malicet,

Absorption spectra measurements for the ozone molecule in the 350-830 nm region, J. Atmos. Chem. 30 (1998) 291–299. doi:10.1023/A:1006036924364.

[9] D. Bertagna Silva, A. Cruz-Alcalde, C. Sans, J. Giménez, S. Esplugas, Performance and kinetic modelling of photolytic and photocatalytic ozonation for enhanced micropollutants removal in municipal wastewaters, Appl. Catal. B Environ. 249 (2019) 211–217. doi:10.1016/j.apcatb.2019.02.072.

[10] F.J. Rivas, R.R. Solís, F.J. Beltrán, O. Gimeno, Sunlight driven photolytic ozonation as an advanced oxidation process in the oxidation of bezafibrate, cotinine and iopamidol, Water Res. 151 (2019) 226–242. https://www.sciencedirect.com/science/article/pii/S0043135418310285 (accessed March 26, 2019).

[11] R.R. Solís, S. Medina, O. Gimeno, F.J. Beltrán, Solar photolytic ozonation for the removal of recalcitrant herbicides in river water, Sep. Purif. Technol. 212 (2019) 280–288. doi:10.1016/j.seppur.2018.11.035.

[12] L. Erdei, N. Arecrachakul, S. Vigneswaran, A combined photocatalytic slurry reactor–immersed membrane module system for advanced wastewater treatment, Sep. Purif. Technol. 62 (2008) 382–388. doi:10.1016/J.SEPPUR.2008.02.003.

[13] A.M. Chávez, A. Rey, F.J. Beltrán, P.M. Álvarez, Solar photo-ozonation: A novel treatment method for the degradation of water pollutants, J. Hazard. Mater. 317 (2016) 36–43. doi:10.1016/j.jhazmat.2016.05.050.

[14] A.M. Chávez, D.H. Quiñones, A. Rey, F.J. Beltrán, P.M. Álvarez, Simulated solar photocatalytic ozonation of contaminants of emerging concern and effluent organic matter in secondary effluents by a reusable magnetic catalyst, Chem. Eng. J. 398 (2020) 125642. doi:10.1016/j.cej.2020.125642.

[15] F.J. Beltrán, Ozone reaction kinetics for water and wastewater systems, Lewis Publishers, Florida, 2004.

[16] R. Acosta-Herazo, P.J. Valadés-Pelayo, M.A. Mueses, M.H. Pinzón-Cárdenas, C. Arancibia-Bulnes, F. Machuca-Martínez, An optical and energy absorption analysis of the solar compound parabolic collector photoreactor (CPCP): The impact of the radiation distribution on its optimization, Chem. Eng. J. 395 (2020) 125065. doi:10.1016/j.cej.2020.125065.

685 [17] E.M. Rodríguez, G. Fernández, P.M. Álvarez, R. Hernández, F.J. Beltrán,
686 Photocatalytic degradation of organics in water in the presence of iron oxides:
687 Effects of pH and light source, Appl. Catal. B Environ. 102 (2011) 572–583.
688 doi:10.1016/j.apcatb.2010.12.041.

689 [18] J.N. Miller, J.C. Miller, R.D. Miller, Statistics and chemometrics for analytical
690 chemistry, Seventh ed, Pearson Education Limited, Harlow (United Kingdom),
691 2018.

692 [19] H. Bader, J. Hoigné, Determination of ozone in water by the indigo method,
693 Water Res. 15 (1981) 449–456. doi:10.1016/0043-1354(81)90054-3.

694 [20] C.C. David Yao, W.R. Haag, Rate constants for direct reactions of ozone with
695 several drinking water contaminants, Water Res. 25 (1991) 761–773.
696 doi:10.1016/0043-1354(91)90155-J.

697 [21] M.S. Alam, B.S.M. Rao, E. Janata, ·OH reactions with aliphatic alcohols:
698 Evaluation of kinetics by direct optical absorption measurement. A pulse
699 radiolysis study, Radiat. Phys. Chem. 67 (2003) 723–728. doi:10.1016/S0969-
700 806X(03)00310-4.

701 [22] D.S. Wishart, Y.D. Feunang, A.C. Guo, E.J. Lo, A. Marcu, J.R. Grant, T. Sajed,
702 D. Johnson, C. Li, Z. Sayeeda, N. Assempour, I. Iynkkaran, Y. Liu, A.
703 Maciejewski, N. Gale, A. Wilson, L. Chin, R. Cummings, D. Le, A. Pon, C.
704 Knox, M. Wilson, DrugBank 5.0: a major update to the DrugBank database for
705 2018, Nucleic Acids Res. 46 (2018) D1074–D1082. doi:10.1093/nar/gkx1037.

706 [23] M.D. Gurol, S. Nekouinaini, Effect of Organic Substances on Mass Transfer in
707 Bubble Aeration, J. (Water Pollut. Control Fed. 57 (1985) 235–240.
708 doi:10.2307/25042568.

709 [24] A. López-López, J.S. Pic, H. Benbelkacem, H. Debellefontaine, Influence of t-
710 butanol and of pH on hydrodynamic and mass transfer parameters in an
711 ozonation process, Chem. Eng. Process. Process Intensif. 46 (2007) 649–655.
712 doi:10.1016/j.cep.2006.08.010.

713 [25] M.K. Moraveji, B. Sajjadi, R. Davarnejad, S.S. Zade, Influence of butanol
714 addition on mass transfer and bubble diameter in a split-cylindrical airlift reactor,
715 Indian J. Chem. Technol. 18 (2011) 277–283.

716 [26] D.W. van Krevelen, P.J. Hoftijzer, Kinetics of gas-liquid reactions part I. General
717 theory, Recl. Des Trav. Chim. Des Pays-Bas. 67 (1948) 563–586.
718 doi:10.1002/recl.19480670708.

719 [27] P.N. Johnson, R.A. Davis, Diffusivity of Ozone in Water, J. Chem. Eng. Data. 41
720 (1996) 1485–1487. doi:10.1021/je9602125.

721 [28] C.R. Wilke, P. Chang, Correlation of diffusion coefficients in dilute solutions,
722 AIChE J. 1 (1955) 264–270. doi:10.1002/aic.690010222.

723 [29] F.J. Beltrán, A. Aguinaco, J.F. García-Araya, A. Oropesa, Ozone and
724 photocatalytic processes to remove the antibiotic sulfamethoxazole from water,
725 Water Res. 42 (2008) 3799–3808. doi:10.1016/J.WATRES.2008.07.019.

726 [30] A.A. Bletsou, J. Jeon, J. Hollender, E. Archontaki, N.S. Thomaidis, Targeted and
727 non-targeted liquid chromatography-mass spectrometric workflows for
728 identification of transformation products of emerging pollutants in the aquatic
729 environment, TrAC Trends Anal. Chem. 66 (2015) 32–44.
730 https://www.sciencedirect.com/science/article/pii/S0165993615000035 (accessed
731 February 19, 2019).

732 [31] A. Cruz-Alcalde, S. Esplugas, C. Sans, Abatement of ozone-recalcitrant
733 micropollutants during municipal wastewater ozonation: Kinetic modelling and
734 surrogate-based control strategies, Chem. Eng. J. 360 (2019) 1092–1100.
735 doi:10.1016/J.CEJ.2018.10.206.

736 [32] A.S. Crucq, B.L. Tilquin, B. Hickel, Radical mechanisms of cephalosporins: A
737 pulse radiolysis study, Free Radic. Biol. Med. 18 (1995) 841–847.
738 doi:10.1016/0891-5849(94)00204-W.

739 [33] F.J. Rivas, F.J. Beltrán, B. Acedo, Chemical and photochemical degradation of
740 acenaphthylene. Intermediate identification, J. Hazard. Mater. 75 (2000) 89–98.
741 doi:10.1016/S0304-3894(00)00196-5.

742 [34] A.C. Reina, A.B. Martínez-Piernas, Y. Bertakis, C. Brebou, N.P.
743 Xekoukoulotakis, A. Agüera, J.A. Sánchez Pérez, Photochemical degradation of
744 the carbapenem antibiotics imipenem and meropenem in aqueous solutions under
745 solar radiation, Water Res. 128 (2018) 61–70. doi:10.1016/j.watres.2017.10.047.

[35] F.J. Beltrán, G. Ovejero, J.F. García-Araya, J. Rivas, Oxidation of Polynuclear Aromatic Hydrocarbons in Water. 2. UV Radiation and Ozonation in the Presence of UV Radiation, Ind. Eng. Chem. Res. 34 (1995) 1607–1615. doi:10.1021/ie00044a013.

[36] X.H. Wang, A.Y.C. Lin, Phototransformation of cephalosporin antibiotics in an aqueous environment results in higher toxicity, Environ. Sci. Technol. 46 (2012) 12417–12426. doi:10.1021/es301929e.

[37] J. Hoigné, H. Bader, Rate constants of reactions of ozone with organic and inorganic compounds in water—II: Dissociating organic compounds, Water Res. 17 (1983) 185–194. doi:10.1016/0043-1354(83)90099-4.

[38] F.J. Beltrán, A. Aguinaco, J.F. García-Araya, Mechanism and kinetics of sulfamethoxazole photocatalytic ozonation in water, Water Res. 43 (2009) 1359–1369. doi:10.1016/j.watres.2008.12.015.

[39] C. Liang, C. Anastasio, Formation of hydroxyl radical from the photolysis of frozen hydrogen peroxide , J. Phys. Chem. A. 112 (2008) 2747–2748. doi:10.1021/jp800491n.